# Spatio-Temporal Characteristics of Filamentation in Broad-Area Semiconductor Lasers

John R. Marciante and Govind P. Agrawal, *Fellow, IEEE*

***Abstract*—Using the time-dependent rate equations appropriate for semiconductor lasers, we perform a linear stability analysis to derive an analytic expression for the filament gain as a function of the filament spacing, oscillation frequency, linewidth-enhancement factor, pumping level, and nonlinear refractive index. The spatio-temporal characteristics of filamentation are obtained for a given set of operating parameters by maximizing the filament gain. Our theory predicts that there is a critical value of the linewidth-enhancement factor below which broad-area lasers remain stable even at high pumping levels. Moreover, under certain conditions, the self-defocusing Kerr-type nonlinearity can be used to suppress filamentation even when the linewidth-enhancement factor exceeds this critical value.**

***Index Terms*—Beam filmentation, broad-area lasers, dynamics, laser stability, optical propagation in nonlinear media, semiconductor lasers, spatio-temporal instabilities.**

## I. Introduction

FOR MANY YEARS, the availability of high-power semiconductor lasers has been hampered by the phenomenon of beam filamentation [1]–[9]. For broad-area gain regions, since the light has no lateral confinement, any increase in the local refractive index can lead to self-focusing, breaking up the lateral mode profile into multiple filaments. Amplifier and MOPA configurations have been used to counteract this problem, but filamentation eventually limits the device performance and output power [1], [2]. Recent theoretical studies have discussed the growth and formation of filamentation in broad-area semiconductor laser amplifiers [3]–[6], and some numerical work has covered the issues of filamentation threshold [7] and spatio-temporal chaos [8], [9] in semiconductor lasers. However, an analytical study capable of predicting the spatio-temporal characteristics of filamentation is still lacking.

In this paper, we present a theoretical analysis of the spatio-temporal nature of filamentation in broad-area semiconductor lasers. Our work differs from previous work [3] in that we include time dependence and perform our analysis for a semiconductor laser rather than an amplifier. We derive an expression for the perturbative filament gain through the semiconductor-laser rate equations by using a linear stability analysis. From this expression, which includes parametric dependence on the filament spacing and oscillation frequency, the linewidth-enhancement factor, the current injection level, and the nonlinear refractive index, we can locate the global maximum and predict the spatio-temporal characteristics of filamentation for a given set of operating parameters.

This paper is organized as follows. In Section II, we present the nonlinear coupled differential rate equations for a semiconductor laser and derive their steady-state solution. Section III continues with a linear stability analysis of these equations to derive a functional form for the perturbative filament gain. In Section IV, we analyze this gain function to obtain the spatio-temporal filamentation characteristics as a function of the linewidth-enhancement factor and pumping level. We also study the effects of a Kerr nonlinearity introduced through the nonlinear refractive index. Section V is devoted to the discussion and conclusions of our main results.

## II. Theoretical Model and Steady-State Solution

In mathematically describing a semiconductor laser, several approximations are made. First, we consider an infinitely wide current stripe. This has the implications of not being able to predict effects due to the edges of the current injection stripe, the ramifications of which shall be discussed in Section IV. Second, to avoid solving a complicated boundary-value problem, we assume that mirror losses are distributed throughout the cavity. We consider field propagation only in the forward direction by unfolding the Fabry–Perot cavity and assume that the intracavity intensity $|E|^2$ changes slowly along $z$. The intracavity field then satisfies the paraxial wave equation [10]

$$\frac{\partial E}{\partial z}+\frac{1}{v_g}\frac{\partial E}{\partial t}=\frac{i}{2k}\frac{\partial^2 E}{\partial x^2}+\left[\frac{1}{2}\Gamma(1-i\alpha)g(N)-\frac{a_{\rm cav}}{2}+in_2k_0|E|^2\right]E \tag{1}$$

where $v_g$ is the group velocity, $k=n_{\rm eff}k_0$ is the mode-propagation constant, $n_{\rm eff}$ is the effective index of refraction, $k_0=\omega/c$ is the free-space propagation constant, $\Gamma$ is the transverse confinement factor, $\alpha$ is the linewidth-enhancement factor, $\alpha_{\rm cav}=\alpha_{\rm int}+\ln(R_1R_2)/2L$ represents the distributed cavity loss, $\alpha_{\rm int}$ is the internal loss, $L$ is the cavity length, $R_1$ and $R_2$ are the facet reflectivities, $n_2$ is the Kerr coefficient [11], and $g(N)$ is the local gain assumed to vary with the carrier density $N$ as $g(N)=a(N-N_0)$. Here, $a$ is the gain cross section and $N_0$ is the transparency value for the carrier density ($g=0$ at $N=N_0$). Equation (1)

Manuscript received July 19, 1996; revised January 27, 1997. This work was supported in part by the Army Research Office under the University Research Initiative Program.

J. R. Marciante was with the Institute of Optics, University of Rochester, Rochester, NY 14627 USA. He is now with the Semiconductor Laser Branch, USAF Phillips Laboratory, Kirtland AFB, NM 87117-5776 USA.

G. P. Agrawal is with the Institute of Optics, University of Rochester, Rochester, NY 14627 USA.

Publisher Item Identifier S 0018-9197(97)04713-1.

0018–9197/97$10.00 © 1997 IEEE

includes diffraction, carrier-induced index variations, free-carrier absorption, material gain, and self-focusing ($n_2 > 0$) or self-defocusing ($n_2 < 0$) through a Kerr-type nonlinearity. Note that $n_2$ is the effective Kerr coefficient of the waveguide mode and has the general form $n_2 = \Gamma n_2^{\rm act} + (1-\Gamma)n_2^{\rm clad}$, where $n_2^{\rm act}$ and $n_2^{\rm clad}$ are the material Kerr coefficients of the active and cladding layers, respectively.

The carrier density distribution can be obtained by solving [12]

$$\frac{\partial N}{\partial t} - D\frac{\partial^2 N}{\partial x^2} = \frac{J}{qd} - \frac{N}{\tau} - \frac{\Gamma g(N)}{\hbar\omega}|E|^2 \tag{2}$$

where $D$ is the diffusion constant, $J$ is the injected current density, $q$ is the magnitude of the electron charge, $d$ is the active-layer thickness, $\tau = (1/\tau_{\rm nr} + BN_{\rm th})^{-1}$ is the carrier lifetime, $\tau_{\rm nr}$ is the nonradiative lifetime, $B$ is the spontaneous-emission coefficient, and $N_{\rm th}$ is the carrier density at which the laser reaches threshold. On the right-hand side of (2), the first term accounts for carrier injection, while the second term accounts for the nonradiative and spontaneous recombinations. The last term is due to stimulated recombination and accounts for gain saturation. The assumptions implicit here are that the carrier density is uniform over the active-layer thickness, and its axial variations occur over length scales much longer than the diffusion length.

Once the device reaches threshold in the steady-state regime, the carrier density becomes clamped at its threshold value, and thus the gain becomes clamped at a value which exactly compensates for the cavity loss [10]. Using this condition and the fact that our assumption of an infinitely wide current stripe dictates that the carrier density be uniform in the $x$ direction, the threshold carrier density under CW operation is given by

$$N_{\rm th} = N_0 + \frac{\alpha_{\rm cav}}{\Gamma a}. \tag{3}$$

Using this expression and neglecting diffraction for an infinitely wide current stripe, we can rewrite the field equation (1) in the steady state as

$$\frac{\partial E}{\partial z} = i[-\tfrac{1}{2}\Gamma\alpha g(N_{\rm th}) + n_2 k_0 |E|^2]E. \tag{4}$$

Since the total intensity (sum for forward and backward propagating waves) is nearly constant [12], we use the mean-field approximation and replace $|E|^2$ in (4) by an average value and obtain the solution $E = \sqrt{I}\exp(i\beta z)$, where $I$ is the intracavity mean-field intensity, and $\beta$ is given by

$$\beta = -\tfrac{1}{2}\Gamma\alpha g(N_{\rm th}) + n_2 k_0 I. \tag{5}$$

Equation (5) shows the change in the propagation constant (and hence the laser frequency) due to carrier injection and the Kerr nonlinearity.

Using the steady-state forms for the field and carrier density, (2) gives an expression that relates the intracavity intensity to the injected current density

$$\frac{J}{qd} = \frac{N_{th}}{\tau} + \frac{\Gamma g(N_{\rm th})}{\hbar\omega} I. \tag{6}$$

Since the intensity is negligible near threshold, we can readily determine the threshold current density $J_{\rm th} = qdN_{\rm th}/\tau$. Combining this with (6) and defining a pump parameter $r = J/J_{\rm th}$, we arrive at a solution for the intracavity intensity in terms of the pumping level $r$ as

$$I = \frac{I_s(r-1)}{\left(1 - \dfrac{N_0}{N_{\rm th}}\right)} \tag{7}$$

where $I_s = \hbar\omega/(\Gamma a\tau)$ is the saturation intensity. As will be seen later, (7) can be used to eliminate the intensity $I$ from our results, replacing it instead with the pumping level $r$, a more practical control parameter.

## III. Linear Stability Analysis and Filament Gain

Before accepting the steady-state solution (7) and concluding that the laser will operate continuously, we must examine the stability of this solution to small perturbations. The steady-state solution is stable if small perturbations decay with time, while their growth signifies that the CW solution (7) is unstable. We follow the standard procedure for linear stability analysis and linearize (1) and (2) in terms of small, perturbative parameters $\varepsilon$ and $n$, defined as $E = [\sqrt{I} + \varepsilon(x, z, t)]\exp(i\beta z)$ and $N = N_{\rm th} + n(x, z, t)$. Linearizing (1) and (2) in $\varepsilon$ and $n$, and using the steady-state solutions, yields the following set of two coupled linear equations:

$$\frac{\partial\varepsilon}{\partial z} + \frac{1}{v_g}\frac{\partial\varepsilon}{\partial t} = \frac{i}{2k}\frac{\partial^2\varepsilon}{\partial x^2} + \frac{1}{2}\Gamma(1 - i\alpha)a\sqrt{I}n + in_2 k_0 I(\varepsilon + \varepsilon^*) \tag{8}$$

$$-\tau\frac{\partial n}{\partial t} + \tau D\frac{\partial^2 n}{\partial x^2} = n\left(1 + \frac{I}{I_s}\right) + \frac{g(N_{\rm th})}{a}\frac{\sqrt{I}}{I_s}(\varepsilon + \varepsilon^*). \tag{9}$$

The linearized equations (8) and (9) can be easily solved by using the Fourier method. Each Fourier component of $\varepsilon$ corresponds to a planewave perturbation of the form $\exp[i(k_x x + k_z z - \Omega t)]$ where $k_x$ is the spatial frequency of the perturbation, $\Omega$ is its oscillation frequency, and $k_z$ is the propagation constant to be determined by solving (8) and (9). Further, we note that since $\varepsilon$ represents a complex field, it is determined by two independent variables, which can be amplitude and phase, real and imaginary parts [3], or complex conjugates [13]. By examination of (8) and (9), the latter seems to be the best choice. By eliminating the carrier density perturbation, we arrive at two coupled algebraic equations for $\varepsilon$ and $\varepsilon^*$. These two homogeneous equations have a nontrivial solution only when $k_z$ is given by

$$k_z = \frac{\Omega}{v_g} + i\frac{G}{2} \pm \sqrt{\frac{k_x^2}{k}\left[\frac{k_x^2}{4k} - \frac{\alpha_{\rm eff}G}{2} - n_2 k_0 I\right] - \frac{G^2}{4}} \tag{10}$$

where the effective value of the linewidth-enhancement factor has been defined as

$$\alpha_{\text{eff}} = \frac{\alpha - \dfrac{\Omega\tau}{\left(1+\dfrac{I}{I_s}+D\tau k_x^2\right)}}{1+\dfrac{\alpha\Omega\tau}{\left(1+\dfrac{I}{I_s}+D\tau k_x^2\right)}} \tag{11}$$

and the saturated power gain is given by

$$G = \Gamma g(N_{\text{th}}) \frac{\dfrac{I}{I_s}\left(1+\dfrac{I}{I_s}+D\tau k_x^2+\alpha\Omega\tau\right)}{\left(1+\dfrac{l}{I_s}+D\tau k_x^2\right)^2+(\Omega\tau)^2}. \tag{12}$$

As seen from (10), $k_z$ is generally complex, with its imaginary part providing gain for the perturbation. However, the steady-state solution remains stable as long as the gain is below the cavity loss level. This is the case, for example, when $k_x = 0$. For other values of $k_x$ and $\Omega$, the gain may exceed the cavity loss, making the perturbative Fourier components grow exponentially with propagation, thereby destabilizing the CW solution. This is the origin of filamentation in semiconductor lasers. We can extract the gain of this instability from the imaginary part of (10) by using $g = -2\text{Im}(k_z)$, where the factor of 2 is used to define power gain, and obtain

$$g = \text{Re}\left\{\sqrt{\frac{2k_x^2}{k}\left[\alpha_{\text{eff}}G + 2n_2k_0I - \frac{k_x^2}{2k}\right]+G^2}\right\} - G. \tag{13}$$

For filamentation to occur, it is clear from (10) that only the negative root will yield positive gain, so the other root has been discarded. The spatial frequency $k_x$ of filamentation is related to the filament spacing $w = 2\pi/k_x$, while a nonzero value of the frequency $\Omega$ implies that the filaments are oscillating in time with a frequency $f = |\Omega|/2\pi$.

Equation (13) describes the gain of the instability as a function of the filament spacing and oscillation frequency, as well as the linewidth-enhancement factor, nonlinear refractive index, and pumping level through (7). By comparing the terms within the radical sign, we can draw several general conclusions. It is readily seen that the filament gain increases with the linewidth-enhancement factor $\alpha$, yet a highly saturated gain will reduce its effect. This feature can be understood by noting that as the gain where the filament is located saturates, the regions surrounding the filament will experience more gain, thereby allowing the surrounding regions to increase in intensity. A similarly combative effect is that of diffraction, as can be noted from the terms under the radical. Moreover, the more closely spaced the filaments are, the larger effect diffraction will have. Thus, we can expect diffraction to play a significant role in determining the filament spacing. Carrier diffusion plays a role similar to both diffraction and gain saturation in that the carriers, which are responsible for the $\alpha$-induced self-focusing, tend to disperse in such a way as to reduce spatial modulations, thus reducing spatial index modulations directly. The nonlinear index $n_2$ can have detrimental or beneficial effects, depending on its sign. It has been shown [7] that positive values of $n_2$ will lead to filamentation through self-focusing, thus enhancing the effect of the linewidth-enhancement factor. However, note that a negative value of this parameter will help to combat filamentation through self-defocusing, thus counteracting the carrier-induced self-focusing governed by the linewidth-enhancement factor. This effect has been noted in several numerical studies which predict the reduction of filamentation tendencies through use of this nonlinear index [7], [14].

The analysis presented here can be applied to a semiconductor amplifier [3] with the following complication. In an amplifier, the intensity increases rapidly along the amplifier length, and the mean-field approximation cannot be made. It is necessary to include the axial variation of the steady-state intensity. The calculation can be performed using an integrated gain $\exp\left[\int_0^z g(z')\,dz'\right]$ instead of $\exp(gz)$. One can then proceed through the calculation as presented here to find a form for the local gain $g(z)$ that is similar to (13). As will be shown in Section IV, the spatio-temporal characteristics of this instability vary as a function of the intracavity intensity. Thus, the local gain $g(z)$ must be integrated along the $z$ axis to obtain the overall filament gain in the amplifier.

## IV. Spatio-Temporal Analysis of Filament Gain

The instability gain given by (13) is a complicated function of many variables. It is useful to consider first the variation of the gain function in the spatio-temporal domain with a fixed set of operating parameters. In general, one should consider both positive and negative values of $\Omega$. However, the instability gain $g(k_x, \Omega)$ has but a single peak occurring at a negative value of $\Omega$, implying that the modulation-type instability will lead to growth of a single sideband on the "red" side of the laser frequency. This is in sharp contrast with the case of optical fibers where the modulation-instability gain spectrum is symmetric in $\Omega$ with a double-peak structure. The difference can be attributed to the nature of the nonlinearities in the two cases. Whereas the Kerr effect is the origin of instability in fibers, it is the gain saturation and the corresponding $\alpha$-induced index nonlinearity that gives rise to a single sideband for semiconductor lasers. Note that the above analysis assumes that the sideband grows from noise (spontaneous modulation instability). In the case of induced modulation instability, corresponding to a four-wave mixing scheme, the injected signal will invariably lead to the growth of a symmetrically situated sideband as long as the instability gain exists.

Using the parameters listed in Table I with $\alpha = 3, r = 2, n_2 = 0$, and $\Omega < 0$, the gain function is displayed in Fig. 1 as a function of the filament spacing $w = 2\pi/k_x$ and the oscillation frequency $f = |\Omega|/2\pi$. Although the surface is complicated, the key feature is that there is an absolute maximum. This maximum will shift in the space–time domain for various parameter variations, namely the linewidth-enhancement factor $\alpha$ and the pump parameter $r$.

The gain function in Fig. 1 has been normalized to the cavity loss $\alpha_{\text{cav}}$. The motivation for this is that for the

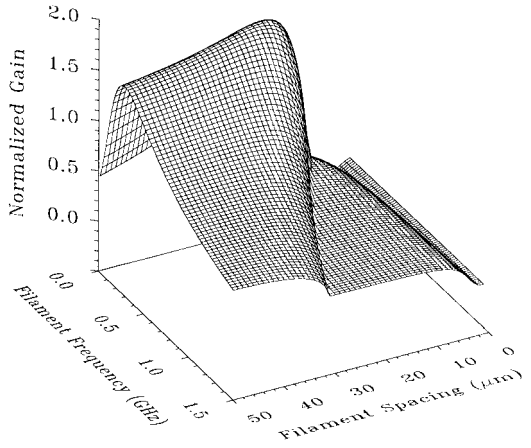


Fig. 1. Perturbative filament gain surface as a function of filament frequency $f$ and spacing $w$ for $\alpha = 3, r = 2$, and $n_2 = 0$. The gain is normalized to the cavity loss $\alpha_{\text{cav}}$.

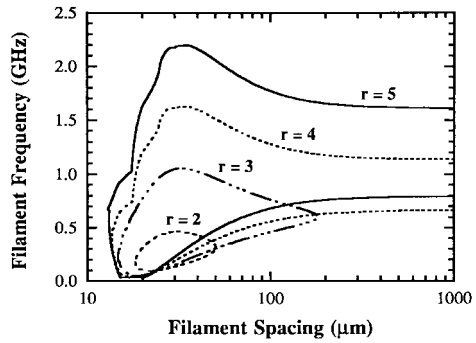


(a)

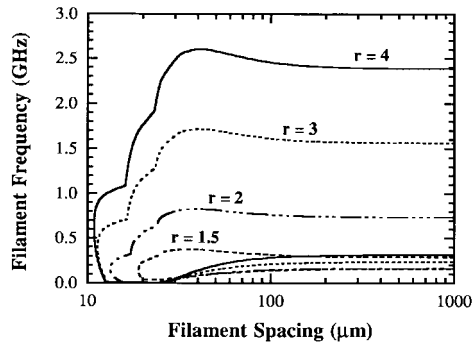


(b)

Fig. 2. Gain contours for which the filament gain equals the cavity loss in the $f$–$w$ plane for various pumping levels $r$: (a) $\alpha = 2$ and (b) $\alpha = 3$. Both cases use a logarithmic scale for the horizontal axis and $n_2 = 0$.

filamentation to occur, the filament gain must exceed the cavity loss. Thus, when the normalized gain exceeds unity, the laser will exhibit filamentary behavior. Fig. 1 shows a large portion of the surface where $g > \alpha_{\text{cav}}$. To look at this in more detail, we plot the contours where the instability gain equals the cavity loss. Fig. 2(a) shows these contours for various pump levels where $\alpha = 2$. Filamentation can occur inside the region bounded by the contour. Note that decreased pumping decreases the potential range of the filamentary spatio-temporal characteristics. In fact, for $r = 1.5$, there was no contour for $g = \alpha_{\text{cav}}$, indicating that no filamentation would occur. Fig. 2(b) displays similar contour plots for the

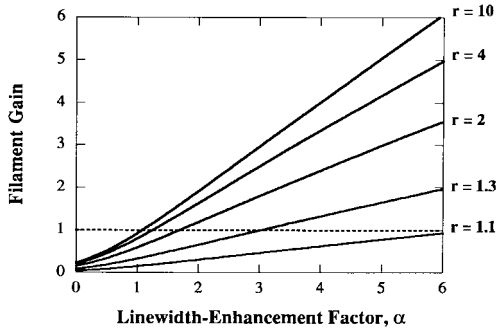


(a)

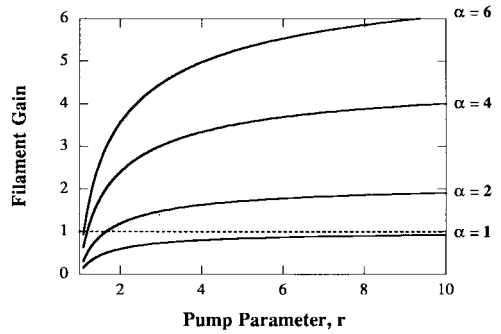


(b)

Fig. 3. Filament gain maxima normalized to the cavity loss $\alpha_{\text{cav}}$: (a) gain versus $\alpha$ for various $r$ and (b) gain versus $r$ for various $\alpha$. In both cases, $n_2 = 0$ and the dashed line represents the cavity loss which the gain must exceed for the laser to exhibit filamentation.

case of $\alpha = 3$. Here, we see an increase in the instability region as compared with the $\alpha = 2$ contours, marking the critical role of the linewidth-enhancement factor in causing filamentation. Another important distinction is that for $\alpha = 3$, the net gain $(g - \alpha_{\text{cav}})$ is positive for filament spacings in excess of 1000 $\mu$m even at low pumping levels.

Figs. 1 and 2 show that the gain can exceed the cavity loss over a wide range of values for $w$ and $f$. What determines the filament spacing and frequency in a given laser? The answer to this question is that the perturbation for which the gain is maximum would grow fastest and would dominate the growth process. It would thus be useful to know how the gain maximum varies with the linewidth-enhancement factor and the pumping level. Fig. 3 displays plots of the peak gain as a function of $\alpha$ and $r$. In these figures, the dashed horizontal line represents the loss level which the filament gain must exceed in order for filamentation to dominate the behavior of the laser. Several points are clear from these figures. Fig. 3(a) shows that for pumping levels just above threshold, no filamentation will take place, as has been noted in practice. Fig. 3(b) shows that there is a value for the linewidth-enhancement factor below which the laser is stable even when pumped ten times above threshold, behavior which has been discovered through simulations as well [7]. From (13), we can infer that this stability region exists with $\alpha > 0$ due to the spreading effects of diffraction, local gain saturation, and carrier diffusion. The physics represented in Fig. 3 indicate that increasing either pumping or the linewidth-enhancement factor will increase the tendency for filamentation, as has also been noted in practice.

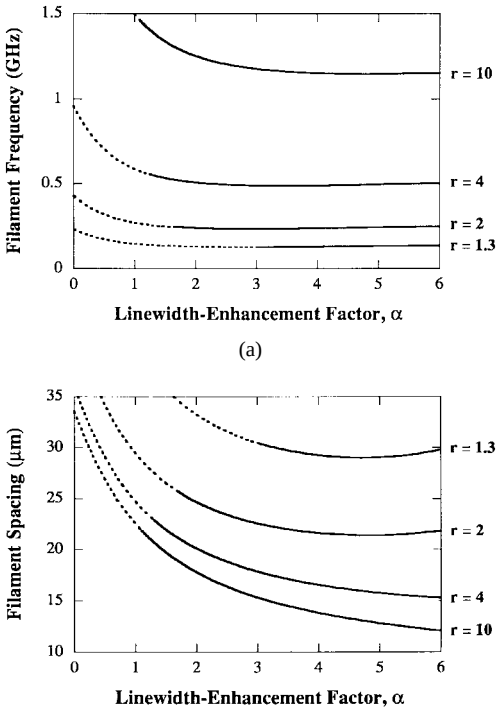


Fig. 4. (a) Filament frequency and (b) filament spacing as a function of the linewidth enhancement factor $\alpha$ for various pumping levels $r$ with $n_2 = 0$. The dashed portions of the curves indicate that the gain is less than the cavity loss and that filamentation will not occur.

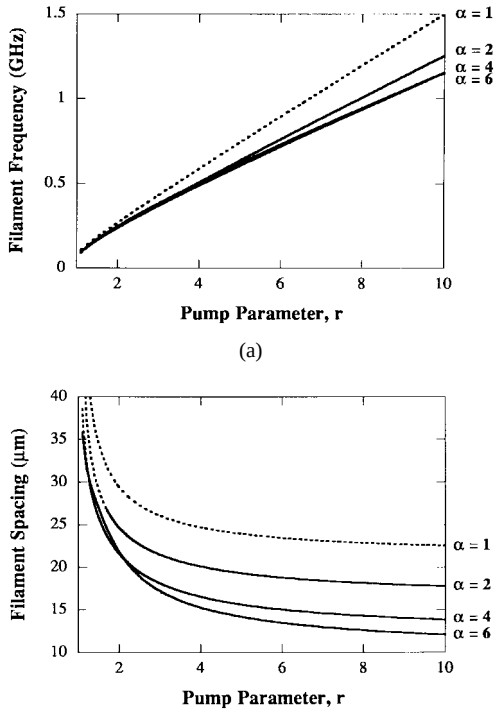


Fig. 5. (a) Filament frequency and (b) filament spacing as a function of the pump level $r$ for various values of the linewidth enhancement factor $\alpha$ with $n_2 = 0$. The dashed portions of the curves indicate that the gain is less than the cavity loss and that filamentation will not occur.

If we operate the laser such that it exhibits filamentary behavior, what information can we obtain about the spatio-temporal nature of this behavior? Each maximum plotted in Fig. 3 occurs at a specific filament spacing $w$ and oscillation frequency $f$. Figs. 4 and 5 plot these spatio-temporal characteristics as a function of $\alpha$ and $r$, respectively. In these plots, the dashed portion of the curves indicates that the gain is less than the cavity loss and that filamentation will not occur. From Fig. 4(a), we note that the oscillation frequency is nearly constant for varying $\alpha$ when the laser exhibits filamentary behavior, but that it increases with pumping level. Fig. 4(b) shows that, in general, the filament spacing decreases with $\alpha$. This behavior will become significant as the spacing approaches the stripe width, which limits the lateral gain dimension. We also note from these plots that increasing the pumping level decreases the filament spacing. The insight from the physical dimensions of the filamentation seems to agree with that of the gain: increased $\alpha$ or $r$ increases the severity of the filamentation.

Fig. 5(a) shows nearly linear dependence of the filament frequency on the pump parameter $r$, with virtually no dependence on $\alpha$ This seems to be another indication of the increased severity of filamentation with pump, but also that the pump is the primary control of the filament oscillation. Fig. 5(b) displays the same behavior as predicted from Fig 4(b) in the decreased filament spacing with increasing $\alpha$ and $r$.

So far, we have predicted the spatio-temporal nature of the filamentation, and predicted regions in the $\alpha - r$ parameter space where the laser will be free of filamentation. As alluded to earlier in Section III, the effect of the nonlinear index of refraction can be beneficial or detrimental, depending on its sign. Gain saturation induces a local increase in the refractive index due to the linewidth-enhancement factor, as can be seen from (2). Through the Kerr nonlinearity, this $\alpha$-induced self-focusing can then be either enhanced by self-focusing ($n_2 > 0$) or reduced by self-defocusing ($n_2 < 0$). Fig. 6 displays the spatio-temporal characteristics for a laser with $\alpha = 2$ and a varying value of $n_2$ for various pumping levels. It is readily seen that the effects of a positive nonlinear index are similar to those caused by increasing $\alpha$: the filaments become more tightly spaced and the oscillation frequency remains nearly constant. The interesting behavior appears when $n_2 < 0$. For small values, self-defocusing has the same effect as reducing $\alpha$ by increasing the filament spacing and slightly increasing the frequency. However, as the self-defocusing become stronger, we notice that there is a transition to a large spacing, as seen in Fig 6(b). The model predicts filament spacings $>1$ mm, values which are larger than typical stripe widths ($\sim$100 $\mu$m) of broad-area lasers. What the rapid rise in filament spacing indicates is that there can only be one filament under the current stripe, hence unfilamented, single-lateral-mode behavior. These results must be used with caution because of our assumption of an infinitely wide stripe. However, numerical simulations for finite-stripe-width lasers have shown qualitatively similar results as far as the transition to stability is concerned [14], and the quantitative discrepancies can be linked to the approximations involved in our model; a more accurate treatment should solve the forward

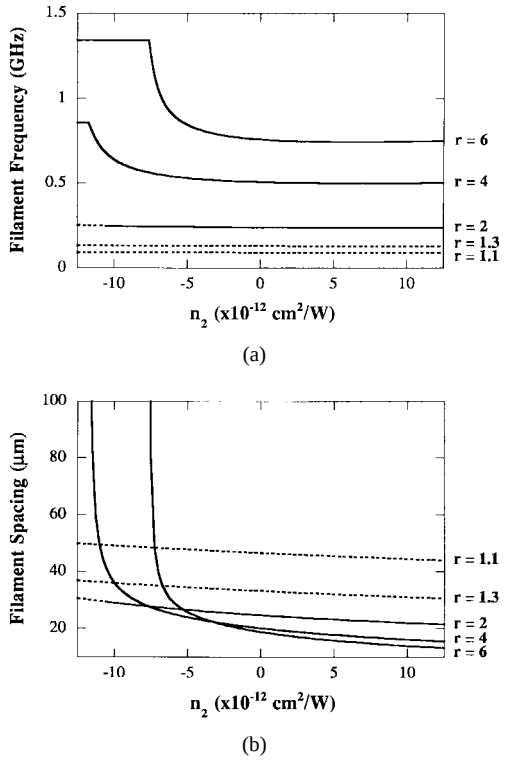


Fig. 6. (a) Filament frequency and (b) filament spacing as a function of $n_2$ for various pumping levels $r$ with $\alpha = 2$. The dashed portions of the curves indicate that the gain is less than the cavity loss and that filamentation will not occur.

and backward wave equations simultaneously [7], [14]. This fact may also be coupled to the instabilities inherent in the self-defocusing nonlinearity at large intracavity intensities [7] in producing oscillatory behavior with a nonfilamented lateral profile. Although the study in [14] described a stable lateral profile, a time-dependent numerical study is necessary to fully determine the temporal characteristics within this self-defocusing-induced stability region. From a practical point of view, the negative values of $n_2$ can be large enough in semiconductor materials [15], [16] to warrant the use of self-defocusing as a means of removing filamentation tendencies of broad-area semiconductor lasers [14].

## V. Conclusion

From a linear stability analysis of the time-dependent semiconductor laser rate equations, we have derived an analytic expression for the filament gain that can be used to predict the spatio-temporal characteristics of filamentation in broad-area lasers. The filament gain function includes dependence on the filament spacing and oscillation frequency, the linewidth-enhancement factor, the pumping level, and the nonlinear refractive index.

We have studied the maxima of the gain function to predict and understand the spatio-temporal characteristics of filamentation and its dependence on the linewidth-enhancement factor and current injection. We have verified that there is a value for the linewidth-enhancement factor below which broad-area lasers are stable even at high pumping levels and explained the physical origin of this stability. We have also shown that lateral instabilities are affected by the Kerr-type nonlinearity which can either enhance or counteract the effects of the carrier-induced index changes, and that this nonlinearity can be used to suppress filamentation caused by the linewidth-enhancement factor.

## References

[1] L. Goldberg, M. R. Surette, and D. Mehuys, "Filament formation in tapered GaAlAs optical amplifier," *Appl. Phys. Lett.*, vol. 62, pp. 2304–2306, 1993.

[2] D. J. Bossert, J. R. Marciante, and M. W. Wright, "Feedback effects in tapered broad area semiconductor lasers and amplifiers," *IEEE Photon. Technol. Lett.*, vol. 7, pp. 470–472, 1995.

[3] A. H. Paxton and G. C. Dente, "Filament formation in semiconductor laser gain regions," *J. Appl. Phys.*, vol. 70, pp. 1–6, 1991.

[4] M. Tamburrini, L. Goldberg, and D. Mehuys, "Periodic filaments in reflective broad area semiconductor optical amplifiers," *Appl. Phys. Lett.*, vol. 60, pp. 1292–1294, 1992.

[5] R. J. Lang, D. Mehuys, A. Hardy, K. M. Dzurko, and D. F. Welch, "Spatial evolution of filaments in broad area diode laser amplifiers," *Appl. Phys. Lett.*, vol. 62, pp. 1209–1211, 1993.

[6] R. J. Lang, D. Mehuys, D. F. Welch, and L. Goldberg, "Spontaneous filamentation in broad-area diode laser amplifiers," *IEEE J. Quantum Electron.*, vol. 30, pp. 685–693, 1994.

[7] J. R. Marciante and G. P. Agrawal, "Nonlinear mechanisms of filamentation in broad-area semiconductor lasers," *IEEE J. Quantum Electron.*, vol. 32, pp. 590–596, 1996.

[8] H. Adachihara, O. Hess, E. Abraham, P. Ru, and J. V. Moloney, "Spatiotemporal chaos in broad-area semiconductor lasers," *J. Opt. Soc. Amer. B*, vol. 10, pp. 658–665, 1993.

[9] O. Hess, S. W. Koch, and J. V. Moloney, "Filamentation and beam propagation in broad-area semiconductor lasers," *IEEE J. Quantum Electron.*, vol. 31, pp. 35–43, 1995.

[10] G. P. Agrawal and N. K. Dutta, *Semiconductor Lasers*, 2nd ed. New York: Van Nostrand Reinhold, 1993.

[11] N. Peyghambarian, S. W. Koch, and A. Mysyrowicz, *Introduction to Semiconductor Optics.* Englewood Cliffs, NJ: Prentice-Hall, 1993, pp. 340–342.

[12] G. P. Agrawal, "Fast-Fourier-transform based beam-propagation model for stripe-geometry semiconductor lasers: Inclusion of axial effects," *J. Appl. Phys.*, vol. 56, pp. 3100–3109, 1984.

[13] C.-J. Chen, P. K. A. Wai, and C. R. Menyuk, "Self-starting of passively mode-locked lasers with fast saturable absorbers," *Opt. Lett.*, vol. 20, pp. 350–352, 1995.

[14] J. R. Marciante and G. P. Agrawal, "Controlling filamentation in broad-area semiconductor lasers and amplifiers," *Appl. Phys. Lett.*, vol. 69, pp. 593–595, 1996.

[15] M. J. LaGasse, K. K. Anderson, C. A. Wang, H. A. Haus, and J. G. Fujimoto, "Femtosecond measurements of the nonresonant nonlinear index in AlGaAs," *Appl. Phys. Lett.*, vol. 56, pp. 417–419, 1990.

[16] K. L. Hall, A. M. Darwish, E. P. Ippen, U. Koren, and G. Raybon, "Femtosecond index nonlinearities in InGaAsP optical amplifiers," *Appl. Phys. Lett.*, vol. 62, pp. 1320–1322, 1993.

**John R. Marciante** received the B.S. degree in engineering physics from the University of Illinois at Urbana-Champaign in 1991 and the M.S. and Ph.D. degrees, both in optics, from the University of Rochester, Rochester, NY, in 1992 and 1997, respectively. His doctoral dissertation work focused on spatial phenomena in semiconductor lasers, namely the study and control of dynamic beam filamentation and spatial effects of optically injected feedback.

After receiving the B.S. degree, he joined Philips Laboratory, Kirtland AFB, NM, under the Palace Knight program, working in the Semiconductor Laser Branch, before beginning his Ph.D. work. He is currently a Research Physicist in the Semiconductor Laser Branch, where his research interests include high-power semiconductor and solid-state laser systems, quantum optics, and nonlinear optics.

Dr. Marciante is a member of the Optical Society of America.

**Govind P. Agrawal** (M'83–SM'86–F'96), for photograph and biography, see p. 468 of the March 1997 issue of this Journal.